

Chemical Science

Accepted Manuscript



This is an *Accepted Manuscript*, which has been through the Royal Society of Chemistry peer review process and has been accepted for publication.

Accepted Manuscripts are published online shortly after acceptance, before technical editing, formatting and proof reading. Using this free service, authors can make their results available to the community, in citable form, before we publish the edited article. We will replace this *Accepted Manuscript* with the edited and formatted *Advance Article* as soon as it is available.

You can find more information about *Accepted Manuscripts* in the [Information for Authors](#).

Please note that technical editing may introduce minor changes to the text and/or graphics, which may alter content. The journal's standard [Terms & Conditions](#) and the [Ethical guidelines](#) still apply. In no event shall the Royal Society of Chemistry be held responsible for any errors or omissions in this *Accepted Manuscript* or any consequences arising from the use of any information it contains.



www.rsc.org/chemicalscience



Journal Name

ARTICLE

Naphthalenebisimides as Photofunctional Surfactants for SWCNTs – Towards Water-Soluble Electron Donor-Acceptor Hybrids

Konstantin Dirian,^{a,†} Susanne Backes,^{a,†} Claudia Backes,^b Volker Strauss,^a Fabian Rodler,^a Frank Hauke,^a Andreas Hirsch^a and Dirk M. Guldi^a

Received 00th January 20xx,
Accepted 00th January 20xx

DOI: 10.1039/x0xx00000x

www.rsc.org/

A water soluble naphthalenebismide derivative (NBI) was synthesized and probed to individualize, suspend, and stabilize single wall carbon nanotubes (SWCNT). Besides a comprehensive photophysical and electrochemical characterization of NBI, stable suspensions of SWCNTs were realized in buffered D₂O. Overall, the dispersion efficiency of the NBI surfactants was determined by comparison with naphthalene based references. Successful individualization of SWCNTs was corroborated in several microscopic assays. In addition, emission spectroscopy points to the strong quenching of SWCNT centered band gap emission, when NBIs are immobilized onto SWCNTs. The origin of the quenching was found to be strong electronic communication, which leads to charge separation from NBI to photoexcited SWCNTs, and, which yields reduced NBI as well oxidized SWCNT. Notably, electrochemical considerations revealed that the energy content of these charged separated states is one of the highest reported for SWCNT based electron donor-acceptor hybrids so far.

Introduction

Ever since their discovery and their large scale production in the 1990's,¹ single wall carbon nanotubes (SWCNT) emerged as benchmark materials in the fields of materials science,² molecular electronics,³ catalysis,⁴ and solar energy conversion.⁵ High performance SWCNT materials mandate to process, to individualize, and to stabilize them, for example, in the form of suspensions. To this date, any of the aforementioned aspects still remains a challenge, since SWCNTs tend to form bundles / ropes due to strong van der Waals interactions.⁶ One way to overcome this intrinsic feature implies the covalent attachment of solubilizing and / or individualizing groups by means of chemical functionalization. Covalent functionalization leads, however, to the transformation of sp² into sp³ hybridized carbons and, in turn, to a notable perturbation of their electronic structure.⁷ An alternative means to ensure processing, individualization, and stabilization, on one hand, and preserving the intrinsic properties of SWCNTs, on the other hand, is their non-covalent functionalization. In this context, a class of promising materials are amphiphiles such as ionic and non-ionic surfactants.⁸

A careful tuning and / or modification of these amphiphilic building blocks targets at the implementation of additional π -systems, electron donors, electron acceptors, etc. A common denominator of the aforementioned is the gain of control over interactions with SWCNTs. For example, considering the extended π -system of SWCNTs and their *p*-type semiconducting nature, an amphiphile featuring an extended, electron accepting π -system should enhance / maximize the stability of SWCNT suspensions. Organic rylene derivatives are promising candidates owing to their susceptibility in terms of charge transfer interactions.⁹ As a matter of fact, perylenebisimides (PBI) have been successfully utilized towards the realization of SWCNT/PBI based electron donor acceptor hybrids, for which experimental data corroborates even in the dark, that is, in the ground state, a redistribution of electron density evoking the partial oxidation of SWCNTs and reduction of PBIs.¹⁰

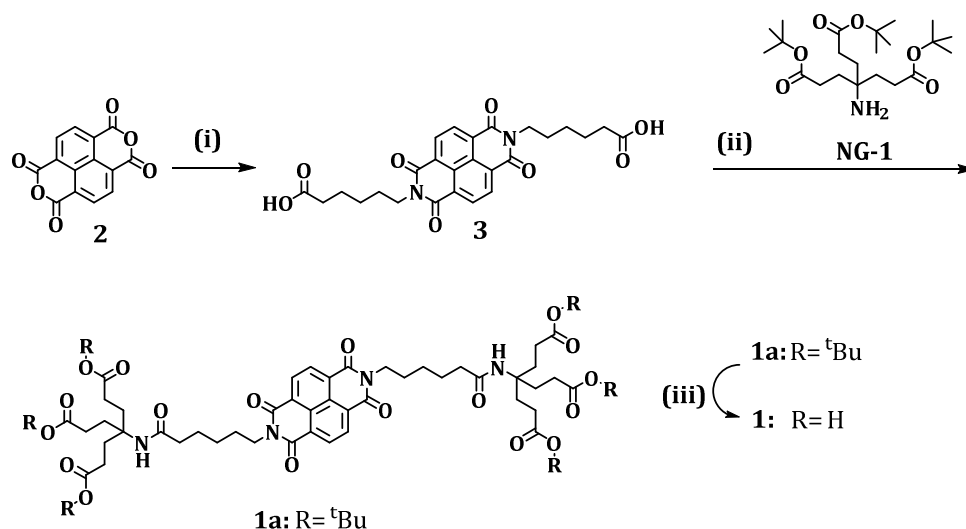
Contrary to PBIs, naphthalenebisimides (NBIs) as the smallest analogue of the rylene family, have rarely been integrated into organic, functional hybrids based on SWCNTs.¹¹ Despite their smaller size, NBI's interesting features such as being a *n*-type semiconductor and exhibiting high π -acidity and chemical versatility renders them promising candidates for novel photoactive SWCNT based hybrids, yielding oxidized SWCNTs as well as reduced NBIs upon illumination or even in the dark.¹² Some of these properties have been proven upon implementing NBIs as electron acceptors into photoactive electron donor-acceptor hybrids,¹³ anion transport¹⁴ as well as electron conducting channels¹⁵ and layers or even π -catalysis.¹⁶

^a Department of Chemistry and Pharmacy and Interdisciplinary Center for Molecular Materials, Friedrich-Alexander-Universität Erlangen-Nürnberg, 91058 Erlangen, Germany

^b School of Physics, Trinity College Dublin, Dublin 2, Ireland

† K. Dirian and S. Backes contributed equally to this work.

Electronic Supplementary Information (ESI) available: [details of any supplementary information available should be included here]. See DOI: 10.1039/x0xx00000x



Scheme 1: Synthesis of NBI 1 (i) 6-aminocaproic acid, toluene/ethanol (1:1), 100 °C, o.n., (ii) 4-(4,6-dimethoxy-1,3,5-triazin-2-yl)-4-methoxymorpholinium chloride, THF, NG-1, 5h, (iii) HCOOH, r.t., 12h.

In this contribution, a water soluble polyanionic NBI (**1**) was used to prepare photoactive HiPco-SWCNT hybrids in aqueous media. By virtue of synergetic effects stemming from hydrophobic / hydrophilic, π - π , and charge transfer interactions, which are operative between **1** and HiPco-SWCNTs, are the basis to individualize HiPco-SWCNTs and to stabilize the corresponding HiPco-SWCNT/**1** suspensions.¹⁷

Results and Discussion

The synthesis of **1** and **1a** is schematically shown in Scheme 1 and the details are provided in the supplementary information (SI).

The first part of our investigations is concerned with the photo- and redoxchemical properties of **1** and its *tert*-butyl protected analogue **1a** as a function of state, that is, monomer *versus* aggregate, in solution (Figure 1). Typically, rylenees are prone to aggregate in solution, which has let us to investigate the aggregation of **1** in D₂O. In the context of **1**, information about its ordering in solution has been gathered in concentration dependent steady state absorption and emission assays.

Figure 1 illustrates that the absorption spectrum of **1** displays – in sound agreement with previous reports – well resolved maxima at 363 and 383 nm and shoulders at 235 and 344 nm with extinction coefficients in the range from 10,000 M⁻¹cm⁻¹ to 20,000 M⁻¹cm⁻¹.^{12a} Interestingly, these features are concentration independent. The latter finding is, however, in stark contrast to investigations with water soluble, *H-type* aggregate forming perylene diimides – see Figure S1.¹⁸ As a complement, 325 nm excitation of **1** resulted in two fluorescence maxima at 395 and 413 nm and in low fluorescence quantum yields in the range of 10⁻⁴.¹⁹ Contrary to the ground state absorption, the fluorescence features of **1** give rise to a concentration dependence. Only at concentrations of less than 10⁻⁵

M the fluorescence appears as mirror image of the ground state absorption, which is shown in Figure 1.

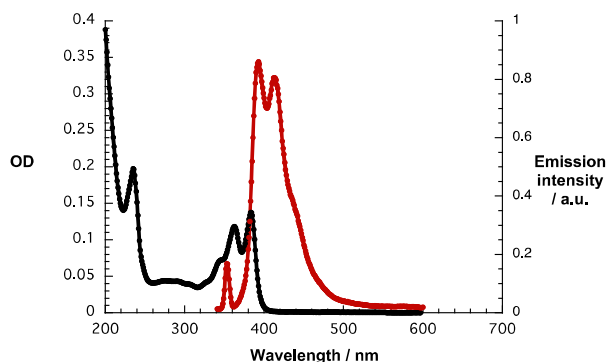


Figure 1: Absorption spectrum (black) and fluorescence spectrum (red) of **1** (7.25×10^{-6} M) in D₂O/H₂PO₄⁻/HPO₄²⁻ upon 325 nm excitation wavelength.

At concentrations of 5×10^{-5} M and higher the long wavelength fluorescence at 413 nm dominates the fluorescence spectrum – Figure S2. In excitation spectra, a good agreement with the absorption features was established as shown in Figure S3. A partial contribution from inner filter effects cannot be ruled out. In additional experiments we probed the influence of ionic strength by addition of sodium chloride as well as of the non-ionic surfactant Triton X. In line with the aforementioned assays, which focused on concentration dependencies, no appreciable alterations of the spectral shape was noted.¹⁸

The energy of the singlet excited state was determined based on the long wavelength absorption and the short wavelength fluorescence maxima as 3.14 eV with a Stokes shift of 0.09 eV.

Owing to the well resolved vibronic fine structure in absorption and fluorescence as well as the small Stokes shift, **1** is unlikely to form *H-type* aggregates. Instead, *J-type* aggregates of **1** or even its monomers – both giving rise to an intrinsically low fluorescence quantum yield – have to be taken into consideration. Notably, weakly fluorescent properties of non-core substituted NBIs have recently been reported.²⁰ Unfortunately, fluorescence lifetime measurements by means of single photon counting rendered impossible due to its low intensity.

Contrary to the fluorescence, phosphorescent features, which are known to center at 605/665 nm (2.05 eV),²¹ could not be detected at room temperature during the course of this study. However, upon purging solutions of **1** in $D_2O/H_2PO_4^-/HPO_4^{2-}$ with oxygen the 1O_2 fluorescence was discernable 1270 nm – Figure 2. With solutions of C_{60} in toluene as standard, the triplet quantum yield of **1** was determined to be around 5%.²²

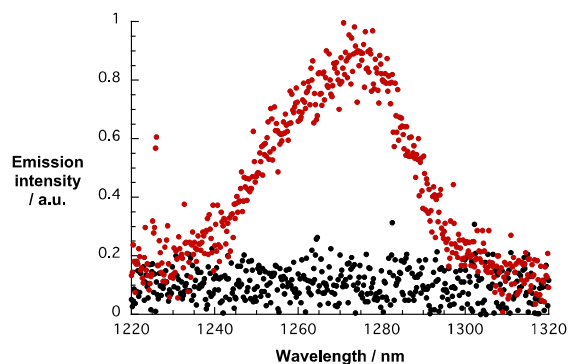


Figure 2: 1O_2 fluorescence spectra of **1** in $D_2O/H_2PO_4^-/HPO_4^{2-}$ (red) with an OD of 0.1 and $D_2O/H_2PO_4^-/HPO_4^{2-}$ (black) upon 360 nm excitation.

Owing to the electron accepting properties of **1**,^{13a,c} we turned to electrochemical and spectroelectrochemical investigations to determine the reduction potentials and the corresponding fingerprints of the one electron reduced form of **1**, respectively. Cyclic voltammetric (CV) and square wave voltammetric (SWV) techniques were used to evaluate the reductions of **1** in $D_2O/H_2PO_4^-/HPO_4^{2-}$ and in DMSO. In $D_2O/H_2PO_4^-/HPO_4^{2-}$, a single, rather irreversible reduction was noted at around -0.6 V vs. $K_3[Fe(CN)_6]/K_4[Fe(CN)_6]$ as shown in Figure 3. In DMSO, two, reversible reductions were observed at -1.1 and -1.5 V vs. Fc/Fc^+ in TBAPF₆,^{15a,23} – Figure S4. Importantly, variable scan rates from 25 to 100 mVs^{-1} lead to identical results – Figure S4. In terms of oxidation, no processes were discernible up to 0.8 V in $D_2O/H_2PO_4^-/HPO_4^{2-}$ and up to 1.3 V in DMSO – both vs. Ag-wire.

In DMSO, on the one hand, application of -0.3 V vs. Ag-wire results in bleaching of the ground state absorption at around 350 nm and in formation of 476 and 607 nm maxima – Figure S5. In $D_2O/H_2PO_4^-/HPO_4^{2-}$, on the other hand, electrochemical reduction of **1** at -0.8 V

vs. Ag-wire is seen to lead to the formation of new maxima in the 400 to 700 nm range, which appear broadened when compared to the DMSO case. An additional feature, which maximizes at 1120 nm, has recently been assigned to arise from π -stacks following reduction – Figure 3.²⁴ As Figure S6 documents these features are reversible throughout at least 3 electrochemical cycles.

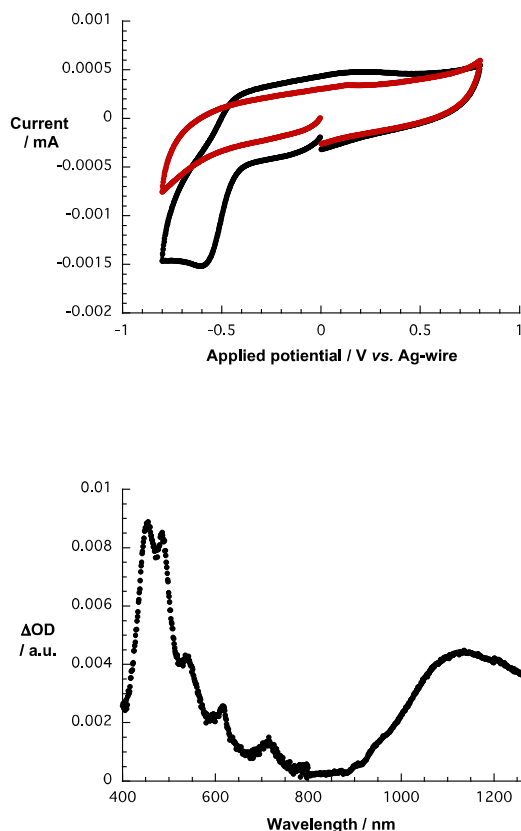


Figure 3: Top: CVs of 5×10^{-4} M **1** in $D_2O/H_2PO_4^-/HPO_4^{2-}$ (black) and $D_2O/H_2PO_4^-/HPO_4^{2-}$ (red) obtained at a 50 mVs^{-1} scan rate. Bottom: Differential absorption spectrum of **1** in $D_2O/H_2PO_4^-/HPO_4^{2-}$ obtained upon electrochemical reduction with an applied potential of -800 mV vs. Ag-wire.

To gather further insights into the excited state dynamics of **1**, femtosecond pump probe experiments were performed by exciting **1** in $D_2O/H_2PO_4^-/HPO_4^{2-}$ at 387 nm. The differential absorption spectra of **1** lack any noticeable transient in the 400 to 1200 nm range, which may be assigned to any singlet excited states, on the femto- and picosecond time scales. When turning, however, to the nano- and microsecond time scales, a transient maximum is noted at 480 nm in stirred and argon purged solutions. Since the corresponding absorption-time profiles reveal decays on the microsecond time range, we tentatively assign the noted transient to the triplet excited state – Figure 4. Confirmation for this hypothesis came from probing its oxygen sensitivity. Taking, for example, the 483 nm time absorption profile a lifetime of 18 μs in argon saturated solution was deduced. Probing oxygen purged

solutions resulted in a sufficient quenching of photoexcited **1**. Now, the lifetime is 680 ns as determined from the 416 nm kinetics.

Reference experiments with **1a** in THF brought a rather different picture – Figure S7. In particular, a strong transient evolves for **1a** at 597 nm within the first few picoseconds following 387 nm excitation. These features transform within less than 15 ps into transient signatures at 450 and 480 nm, which are stable on the 7 ns timescale. Similar transient features have been reported in acetonitrile and assigned to the triplet excited states.²⁵ The triplet nature of these excited states was proven by means of quenching experiments with molecular oxygen on the nano- and microsecond time scale. In the absence of molecular oxygen, a monoexponential decay of, for example, the 482 nm kinetics let to a lifetime of 8.4 μ s. In the presence of oxygen, the lifetime is only 152 ns. The corresponding spectra are gathered in Figure S8. Interestingly, when probing a non stirred solution of **1** in $D_2O/H_2PO_4^-/HPO_4^{2-}$ the differential absorption spectra with a transient centering at 420 nm and the dynamics with a lifetime of 200 μ s – Figure S9 – differ. A likely rationale is based on a photoreaction with the triplet excited state of **1**.

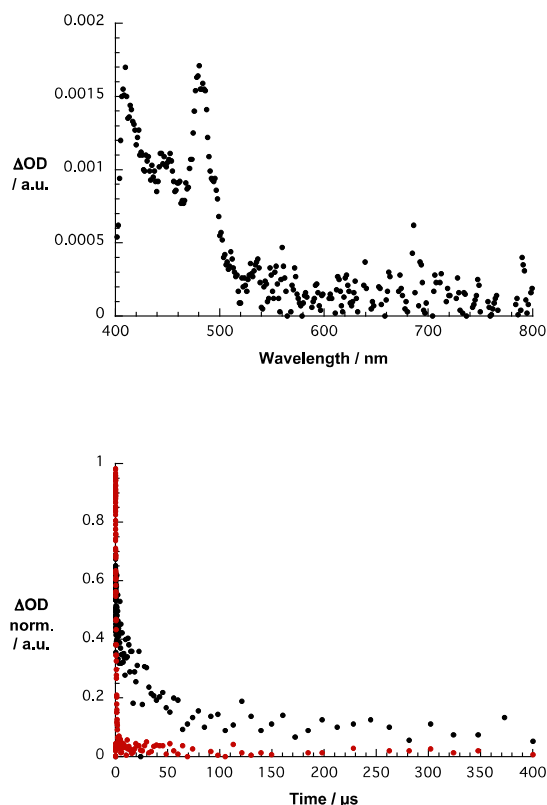


Figure 4: Top: Differential absorption spectrum of **1** in stirred $D_2O/H_2PO_4^-/HPO_4^{2-}$ obtained upon femtosecond flash photolysis (387 nm) with a time delay of 250 ns. Bottom: Time-absorption profile at 483 nm monitoring in the absence (black) and the presence (red) of molecular oxygen monitoring the decay of triplet excited states

Following the characterization of **1** and **1a**, the focus was placed on probing SWCNTs. For the immobilization of **1**, HiPco-SWCNTs were utilized. To study the electronic and photophysical properties of SWCNTs with different chiralities and different band gaps, HiPco-SWCNTs were dispersed in D_2O by surfactant-stabilization with sodium dodecylbenzenesulfonate (SDBS).

The absorption spectrum is best described as the superimposition of several maxima reaching from the visible to the near-infrared – *vide infra* (Figure 8, top). As such, three sets of absorption features are assignable to M_{11} transitions – at wavelengths shorter than 500 nm – to S_{22} transitions – dominating the 500 to 700 nm range – and to S_{11} excitonic transitions – at wavelengths larger than 1000 nm. Assignment of these states to the corresponding SWCNT chiralities is provided in Table S1. Upon photoexcitation in the visible, distinct fluorescence maxima of the S_{11} transitions of different nanotube species were detected in the near-infrared – Figure S10. These findings are well documented and rationalized on the basis of individualized and stabilized SWCNTs, which are, nevertheless, polydisperse.²⁶

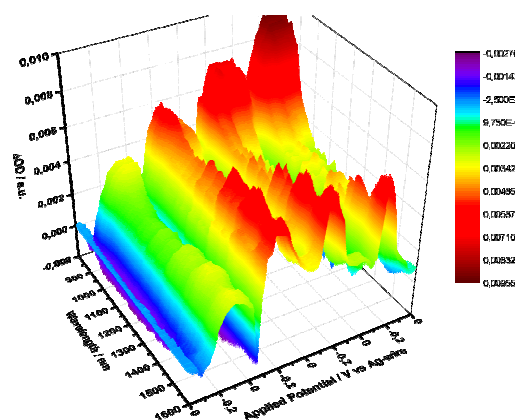


Figure 5: Differential absorption spectra of HiPco-SWCNT/SDBS in $D_2O/0.05$ M NaCl obtained during four electrochemical cycles, that is, from 0 to -800 to +600 and back to 0 mV in 200 mV intervals.

Besides steady-state absorption and fluorescence, Raman spectroscopy is another well established tool to characterize SWCNT dispersions and hybrids.²⁷

For HiPco-SWCNTs solubilized by means of SDBS, Raman analysis upon 1064 nm excitation of the three most important signatures, namely radial breathing modes (RBM), G-, and 2D-modes, was performed and the results were compared to those obtained for solid HiPco-SWCNTs. Importantly, all of the SWCNT modes appear better resolved for HiPco-SWCNT/SDBS. Taking the aforementioned into consideration, we conclude the individualization of HiPco-

SWCNTs.²⁸ The absence of notable electronic communication and / or doping is inferred from the absence of notable shifts in the RBM, G-, and 2D-modes – Table S2 and Figure S11.

Next, the redox properties of HiPco-SWCNT/SDBS were tested utilizing absorption spectroelectrochemistry. Throughout several electrochemical scans, which were performed in the range from -0.8 to +0.6 V vs. Ag-wire, a *quasi* reversible behavior is derived for HiPco-SWCNT/SDBS from absorption vs. potential dependences – Figure 5. Figure S12 gathers the results under oxidative conditions and the resulting potential vs. differential absorption profiles.

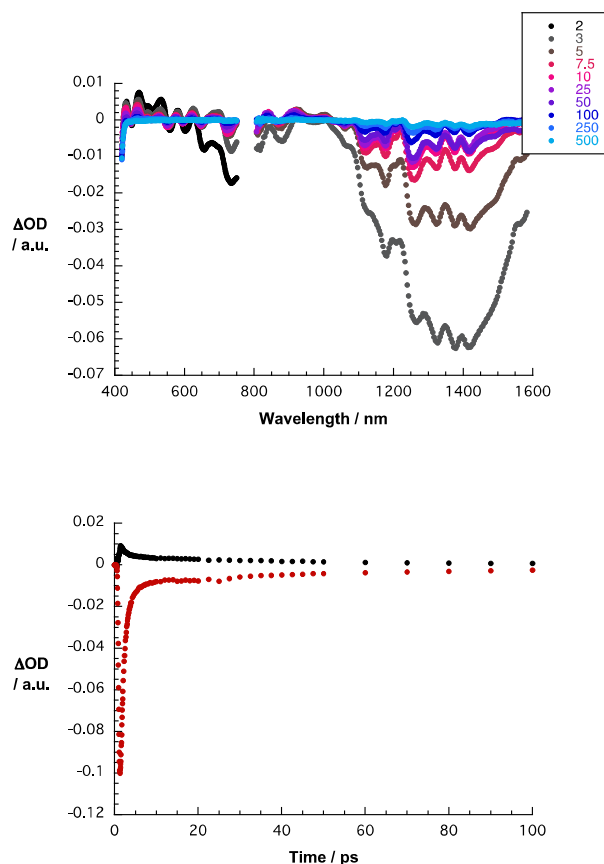


Figure 6: Top: Differential absorption spectra of HiPco-SWCNT/SDBS in D₂O obtained upon femtosecond flash photolysis (387 nm) with time delays between 2 (black) and 500 ps (blue). Bottom: Time absorption profiles at 470 nm (black), and 1323 nm (red), monitoring the excited state decay.

Finally, the excited states of HiPco-SWCNT/SDBS were probed upon 387 nm laser excitation. Immediately after laser excitation, several maxima and minima evolve throughout the visible and near infrared regions. Most prominent is the depopulation of the SWCNT ground state in the form of minima at 1265, 1324, 1378, and 1418 nm as mirror images to the corresponding ground state absorption – S_{11} – Figure 6. From careful kinetic analyses at different wavelengths, a biexponential recovery of the ground state was derived – a short lived, 1 ps component and a longer lived, 50 ps component. Since excitation at 387 nm leads to the population of S_{22} excitonic states,

we assign the short lived component to interband relaxation, whereas the long lived component relates to an excitonic recombination in individualized SWCNTs.²⁹

Following the characterization of **1**, **1a**, and well debundled HiPco-SWCNT, we started optimizing conditions to individualize and to disperse HiPco-SWCNT in the form of HiPco-SWCNT/**1** rather than SWCNT/SDBS. To shed light on the dispersion efficiency of **1**, amphiphilic NBI **4** as well as the corresponding naphthalenemonoimide (NMI, **5**) was probed for comparison – Figure 7. Synthetic details are given in the SI.

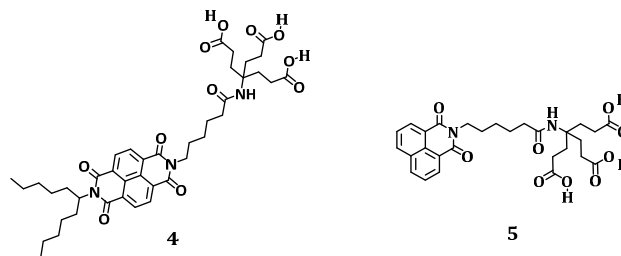


Figure 7: Structures of **4** and **5**.

Perfectly consistent with our previous studies on perylene bisimides (PBI), we find the dispersion efficiency to be significantly higher in buffered systems.³⁰ This is attributed to a higher packing density of the dyes on the nanotubes scaffold due to charge screening by the counterions.³⁰

In the following, we have therefore focused on the investigation of **1** and **4** in buffered media, which are either neutral (pH 7, D₂O/H₂PO₄⁻/HPO₄²⁻) or alkaline (pH 10, H₂O). Notably, decomposition of **1** caused by sonication is ruled out based on NMR data – Figure S13. Stable hybrid materials were, however, obtained only with HiPco-SWCNTs, since attempts to create stable hybrids with CoMoCAT-SWCNTs failed.

A likely rationale is the unbalance between the bulky dendron and the small π skeleton of **1**, reducing π - π interactions between **1** and smaller diameter SWCNTs. Upon comparing the absorption spectra of **1** and HiPco-SWCNT/**1** no appreciable shifts in, for example, the visible range, where NBI centered features dominate, are noted – Figure 8. In the near infrared, a region where SWCNT centered transitions are expected, the latter are for HiPco-SWCNT/**1** strongly broadened and red shifted relative to HiPco-SWCNT/SDBS. The resulting maxima at 1171, 1317, and 1425 nm are assigned to S_{11} transitions of (8,6), (9,4), (8,7), (7,6), and (11,1) HiPco-SWCNT, which are broadened and superimposed as a consequence of the interactions with **1**.

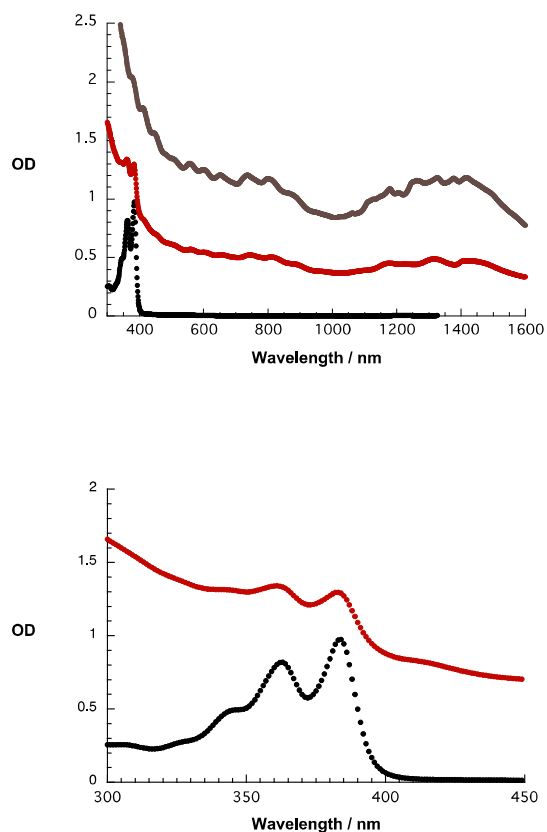


Figure 8: Top: Absorption spectra of **1** (black), HiPco-SWCNT/**1** (red) and HiPco-SWCNT/SDBS (grey) recorded in $D_2O/H_2PO_4^-/HPO_4^{2-}$. Bottom: Zoom into the 300-450 nm range with focus on the absorption features of **1** in HiPco-SWCNT/**1**.

In a complementary approach, the dispersion efficiency of **1** was correlated with that of **4** and **5**, respectively. In pH 10, dispersion efficiencies are derived from the SWCNT concentration in the stable supernatant dispersion – based on the extinction coefficient previously determined³¹ – and the initial SWCNT concentrations. Both **1** and **4** are potent surfactants yielding dispersions, in which typically 60 % of all SWCNTs are effectively dispersed. The related naphthalene monoimide **5** exhibits a significantly lower dispersion efficiency of only 5 % as shown in Figure S14. As a complement to the near infrared absorptions, the near infrared fluorescence of HiPco-SWCNT/**1** was investigated. All throughout the excitation range, that is, from 550 to 775 nm, no appreciable SWCNT related band gap emission evolves. This is consistent with our previous data on perylene bisimide surfactants and documents that the SWCNT fluorescence is quenched and red-shifted when dispersed with **1** and **4**.^{17,30,32} This is, nevertheless, in stark contrast to perylene imidodiester, where the SWCNT fluorescence is not subject to any appreciable quenching.³³ An illustration for HiPco-SWCNT/SDBS and HiPco-SWCNT/**1** without and with additional SDBS is shown in Figure 9, which documents the overall quenching.

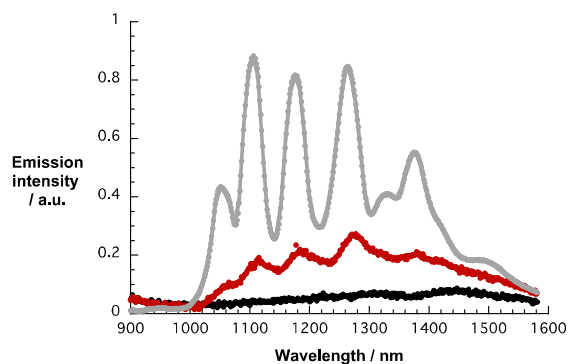


Figure 9: Fluorescence spectra with equal optical density of about 0.4 at the excitation wavelength (724 nm) of HiPco-SWCNT/SDBS (grey), HiPco-SWCNT/**1** (black), and HiPco-SWCNT/**1** after addition of SDBS (red) recorded in $D_2O/H_2PO_4^-/HPO_4^{2-}$. The black and red spectra have been amplified by a factor of 5.

Considering that both effects, namely broadened / red shifted absorption features, on one hand, and strongly quenched fluorescence, on the other hand, may be caused by insufficient debundling³⁴ and / or strong electronic communication^{10a} between HiPco-SWCNT and **1** transmission electron microscopy (TEM) was used to probe the degree of stable individualization in HiPco-SWCNT/**1**. To this end, HiPco-SWCNT/**1** was applied on an ultrathin carbon film covered TEM grid and scanned for individual and bundled objects. The majority of SWCNTs were found to be individualized throughout the entire specimen – Figure 10. To probe the morphology of HiPco-SWCNT/**1**, a high concentrated dispersion of HiPco-SWCNT/**1** was applied on a Lacey carbon film and scanned for freestanding SWCNT networks. As shown in Figure 10 and S15, the freestanding individual SWCNTs feature an amorphous coating that is typical for functionalized or wrapped SWCNTs.

Simultaneously, we performed statistical atomic force microscopic (AFM) analysis of HiPco-SWCNT/**1** alkaline dispersions to corroborate our TEM assays. As shown in Figure 10, the SWCNTs are predominantly individualized. Considering that all the one-dimensional objects with AFM heights <1.5 nm relate to individualized SWCNTs, the degree of individualization is > 65 %. Notably, this is significantly higher than what is typically found when employing SDBS.^{17b,31} From the latter we conclude that the reduced fluorescence intensity in the HiPco-SWCNT/**1** dispersions is due to intermolecular interactions rather than a lack of efficient individualization. The aforementioned assays corroborate the HiPco-SWCNT exfoliation and, in turn, aggregation induced quenching of the fluorescence is ruled out. Consequently, strong electronic communication between HiPco-SWCNT and **1** in form of, for example, charge transfer, are likely to be at force.

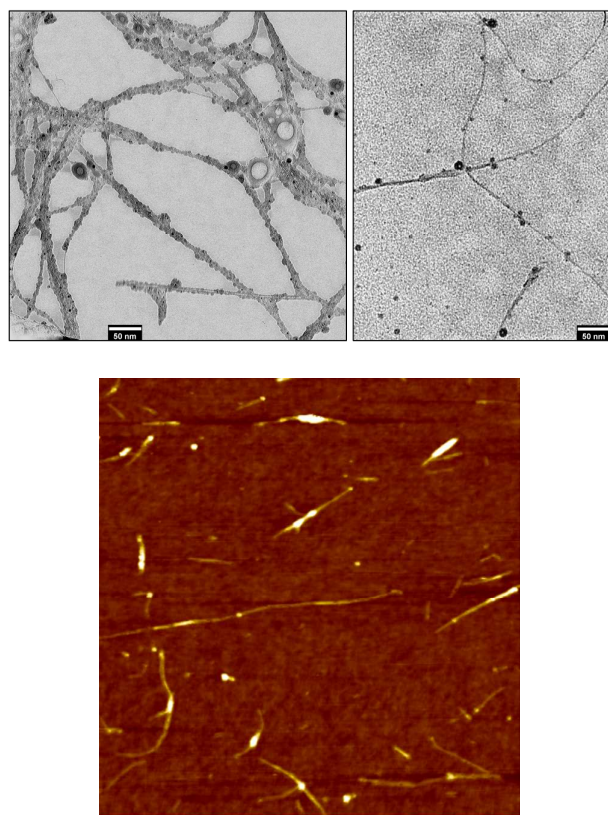


Figure 10: Top: TEM images (80 kV) of freestanding HiPco-SWCNT/1 (left) and on ultrathin carbon film (right) processed from $D_2O/H_2PO_4/HPO_4^{2-}$. Bottom: AFM image of HiPco-SWCNT/1 processed from $H_2O/pH10$.

Further support for this notion came from Raman spectroscopy. Table S2, which lists Raman data for pristine HiPco-SWCNT, HiPco-SWCNT/SDBS, and HiPco-SWCNT/1 taken on alumina substrates, reveal notable differences. Firstly, two Lorentzians are required to appropriately fit the G-mode in HiPco-SWCNT/1. Secondly, the 2D mode – Figure 11 – of HiPco-SWCNT/1 is shifted to $2553\text{ cm}^{-1} \pm 2\text{ cm}^{-1}$ compared to 2550 cm^{-1} for HiPco-SWCNT/SDBS, a finding that infers, for example, a shift of electron density from the electron donating HiPco-SWCNT to the electron accepting **1**, which is in support of charge transfer interactions. For a more comprehensive understanding, Raman spectra, including RBM analysis, of pristine HiPco-SWCNT, HiPco-SWCNT/SDBS and HiPco-SWCNT/1 are shown in Figure S16.³⁵

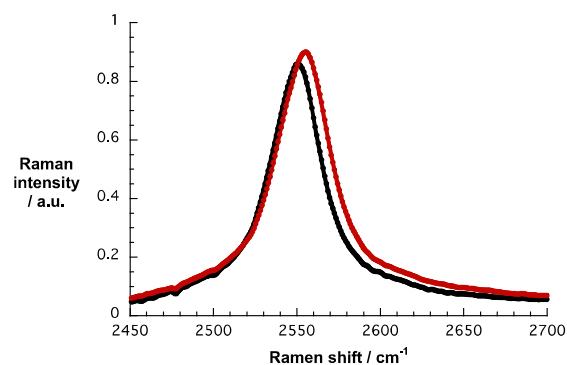
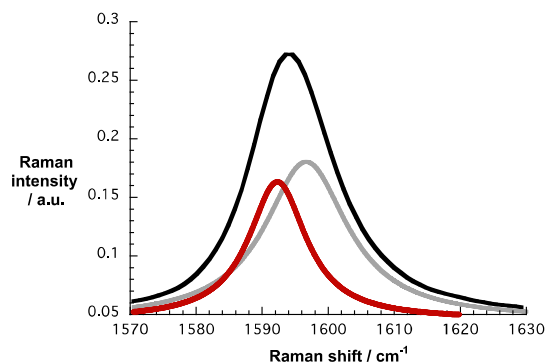


Figure 11: Top: G-band of HiPco-SWCNT/1 upon 1064 nm excitation on alumina substrates and corresponding fit by using two Lorentzian functions. Bottom: Comparison of the 2D-band of HiPco-SWCNT/SDBS (black) and HiPco-SWCNT/1 (red) upon 1064 nm excitation on alumina substrates.

To shed light on the nature of the interactions, which are operative between HiPco-SWCNT and **1**, transient absorption spectroscopic measurements were performed. Immediately following 387 nm pulses, differential absorptions evolve, which differ significantly from those seen for HiPco-SWCNT/SDBS – Figure 12. For HiPco-SWCNT/1, maxima were registered in the visible range at 431, 468, 500, 530, 580, 626, and 680 nm. In stark contrast to HiPco-SWCNT/SDBS, no minima are, however, discernible in this spectral region. Important is in this context that our spectroelectrochemical investigations – *vide supra* – help to document the spectroscopic fingerprints of the one electron reduced form of **1** in this range of the spectrum. Superimposition of these features with the characteristics of HiPco-SWCNT is the origin of the overall spectral shape. Additional evidence for an ultrafast charge transfer was derived from the transient features in the near infrared. In particular, minima, which are noted at 890, 1327, and 1451 nm, are a reflection of the ground state absorption. As time progresses, the aforementioned minima blue shift, that is, from 1327 to 1311 nm and from 1451 to 1442 nm and the underlying transformation is likely due to a charge separation.^{10,35} Thus, we postulate that photoexcitation of HiPco-SWCNT/1 is followed by the formation of

a charge separated state comprised of one electron reduced **1** and oxidized HiPco-SWCNTs. Biexponential kinetic analyses at different wavelength yield lifetimes of 1 and 41 ps, which are assigned to charge separation and charge recombination, respectively – Figure 12.

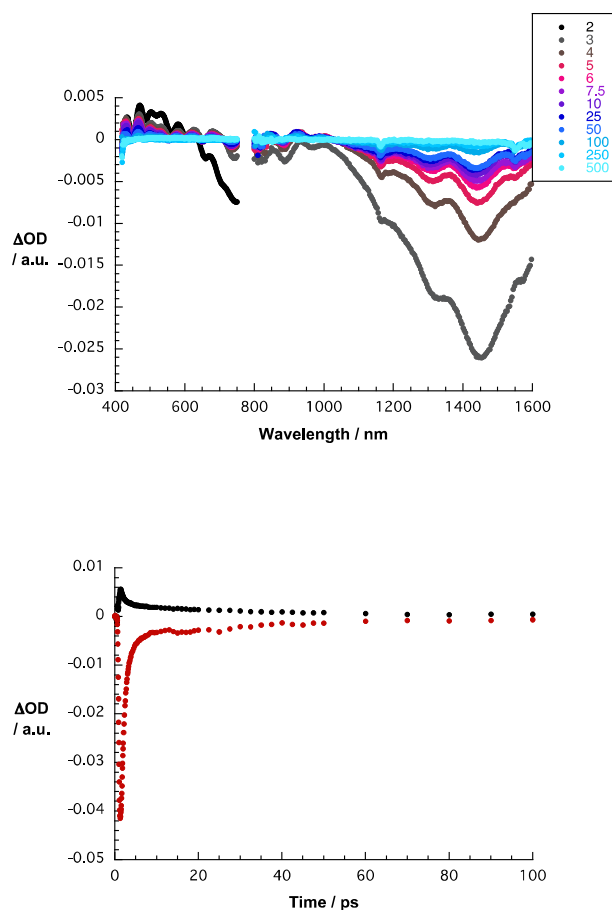


Figure 12: Top: Differential absorption spectra of HiPco-SWCNT/1 in D₂O/H₂PO₄⁻/HPO₄²⁻ obtained upon femtosecond flash photolysis (387 nm) with time delays between 2 (black) and 500 ps (blue). Bottom: Time absorption profiles at 470 nm (black) and 1435 nm (red) monitoring the charge separation and charge recombination.

The electrochemical/spectroelectrochemical experiments assisted in determining the energy of the charge-separated state relative to the ground state. For example, the characteristic features of the one electron reduced form of **1** appear at a potential of -800 mV, whereas the onset of oxidatively induced changes of the E₁₁ and E₂₂ transitions appears in a potential range of +200 and +600 mV, in line with published reports.^{10a,36} Consequently, the energy of the charge separated state ranges from 1.0 to 1.4 eV. Besides localized singlet excited states, which are either HiPco-SWCNT or **1** centered, a charge transfer state is likely the starting point for the charge separation. The corresponding energy values are 3.1 eV for **1** and 1.8 – 2.4 eV for HiPco-SWCNT. We conclude from these considerations that both reduction of **1** and oxidation of SWCNTs are feasible with driving forces of 1.7 – 2.1 and 0.4 – 1.4 eV, respectively – Figure 13. In line with these thermodynamic

arguments is the fact that no evidence is gathered for any triplet excited state.³⁷

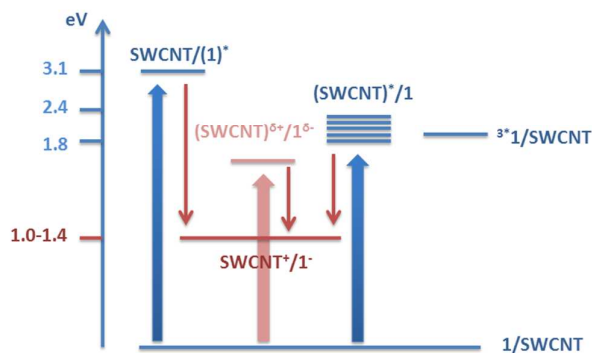


Figure 13: Energy diagram of HiPco-SWCNT/1.

We rounded off our investigation by the selective deimmobilization / removal of either **1** or **4** from SWCNTs. To this end, solid SDBS was added to stable dispersions of HiPco-SWCNT/1 or HiPco-SWCNT/4 and the corresponding spectral changes were monitored by means of steady state absorption, fluorescence, and transient absorption measurements. For a detailed description and analysis the reader is directed in the SI, where data from steady state absorption/emission as well as transient absorption assays are gathered – Figures S17-21.

Materials and methods

Chemicals. TBAPF₆, SDBS and THF were purchased from Sigma Aldrich and used without further purification. DMSO was purchased from Roth chemicals and used without further purification. D₂O was provided by Deutero. To adjust D₂O solutions with pH 7 726 mg Na₂HPO₄ and 352 mg KH₂PO₄ were added to 100 mL D₂O.

Spectroscopy. ¹H and ¹³C NMR spectra were recorded with a Jeol JNM EX 400, Jeol JNM GX (each 400 MHz for ¹H and 100 MHz for ¹³C) and a Jeol Bruker Avance 300 (300MHz for ¹H and 75MHz for ¹³C) spectrometer. Chemical shifts (δ) are reported in ppm at room temperature (r.t.) using CDCl₃ as solvent and internal standard unless otherwise indicated. IR spectra were recorded with an ASI React IR 1000 spectrometer. Mass spectrometry was carried out on a Micromass Zabspec (Cs+) spectrometer with 3-nitrobenzylalcohol (NBA) as matrix in fast atom bombardment (FAB) or on an AXIMA Confidences (Shimadzu) matrix-assisted laser desorption ionization time-of-flight (MALDI-TOF) mass spectrometry (MS) apparatus, respectively. The measurements were carried out in reflectron mode with sin (sinapinic acid) or dhb (2,5-dihydroxybenzoic acid) as matrices. For elemental analyses (EA) a CE instrument EA 1110 CHNS was used. UV/Vis/nIR measurements were performed using either a Perkin Elmer Lambda 2 spectrometer or a Cary 5000 spectrometer (Varian). Emission was detected in the visible range by a Fluoromax3 spectrometer (Horiba Scientific) and in the near infrared by a Fluorolog 3 (Horiba Scientific) equipped with an InGaAs symphony as detection unit.

Transient absorption spectra on the pico- and nanosecond timescale were performed with output from CPA2110 or CPA 2101 Ti/sapphire laser systems from Clark-MXR Inc. (775 nm, 1 kHz, 150 fs FWHM pulses). 387 nm excitation pulses were generated by second harmonic generation. For measurements with pico- and nanosecond time resolution a Helios transient absorption spectrometer was equipped. For the corresponding measurements on the microsecond time scale, a EOS transient absorption spectrometer was used. Both systems were provided by Ultrafast Systems. All measurements were carried out in 2 mm OS quartz cuvettes. Raman spectra were recorded from solid/solid films deposited on alumina pallets. A Bruker Raman spectrometer RFS 100 (nitrogen cooled Ge-detector, $\lambda_{\text{ex}} = 1064 \text{ nm}$) was used for all the experiments.

Microscopy. Transmission electron microscopy was conducted on a Zeiss Leo EM912 Omega with an acceleration voltage of 80 kV. Specimen were prepared by dip casting of either Lacey Carbon/Copper or Lacey Carbon supported ultrathin carbon/Copper grids into a suspension of SWCNT/1 or SWCNT/SDBS. The sample grids were dried at 80 °C for 5 h prior to microscoping.

Atomic force microscopy tapping mode images were recorded on a Solver Pro scanning probe microscope (NT-MDT) equipped with a Sony Exwave HAD camera optical zoom (6.5). The carbon nanotube material was spread on oxidized silicon wafers with a 200 nm thermally grown oxide layer by spin coating (100 rps).

Electrochemistry. Cyclic Voltammetry and Square Wave Voltammetry was performed using a Methrom μ AutobabFrailII with in cooperated impedance unit. Measurements were performed in a homemade cell (V= 5 ml) with a glassy carbon working electrode (3mm diameter), an silver wire acting as pseudo reference electrode and a Pt wire serving as counter electrode. NOVA 1.10[®] from Methrom served as control software.

Spectroelectrochemical measurements were performed in a homemade three neck cell equipped with a Pt-mesh as transparent working electrode, a Ag-wire as pseudo reference electrode and a Pt plate as counter electrode. A PGStat 101 from Methrom was used as potentiostat. The latter was controlled by the software NOVA 1.10[®] provided by Methrom.

Conclusions

In summary, we demonstrated that water soluble NBI **1** is a powerful surfactant to individualize, to stabilize, and to photo-/redoxchemical modulate HiPco-SWCNTs in aqueous media. Our concept to combine π - π , hydrophobic/hydrophilic, and charge transfer interactions, which was earlier established for both perylenebismide/CoMoCAT-SWCNT and perylenebismide/HiPco-SWCNT hybrids,^{10,17} was successfully transferred for the first time to naphthalenebismides yielding stable HiPco-SWCNT/1 hybrids in 0.1M $\text{H}_2\text{PO}_4^-/\text{HPO}_4^{2-}/\text{D}_2\text{O}$. In stark contrast, we failed to generate stable hybrids based on CoMoCAT-SWCNTs due to an unsuitable

balance between the size of the Newkome dendron and that of the naphthalene core. Sequentially, detailed replacement studies with HiPco-SWCNT/1 as well as reference experiments with HiPco-SWCNT/4 and SDBS point to a preferential stabilization of larger diameter SWCNTs with **1** as a result of the packing densities – *vide supra* – Figure 16 and S13.

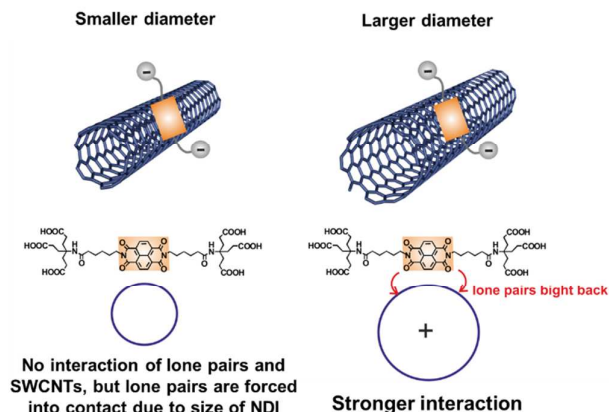


Figure 15: Schematic representation of the mutual orientation of **1** onto HiPco-SWCNT and the resulting interaction.

Besides the comprehensive characterization of **1**, in which we corroborated high energetic, but only moderately emitting excited states together with a strong electron accepting character, ground and excited state interactions between HiPco-SWCNTs and **1** were at the focal point of our investigations. With the help of an arsenal of spectroscopic and microscopic techniques, formation of a charge separated state – comprised of oxidized HiPco-SWCNTs and the one electron reduced form of **1** – was corroborated. The later decays on the picosecond time scale by reinstating the singlet ground state. Notable is the fact that NBIs are among the smallest molecular building blocks, which were ever immobilized onto SWCNTs, and, which afforded stable SWCNT suspensions. In light of their high lying and accessible excited states, **1** forms with HiPco-SWCNTs highly energetic charge separated states (1.2 – 1.4 eV).

Acknowledgements

This work was carried out with support from the DFG throughout SFB 953 “Synthetic Carbon Allotropes”, the Bavarian state throughout the “SolTec” network and the Graduate School of Molecular Science (GSMS) of the University of Erlangen-Nürnberg. Volker Strauss was supported by the “Universität Bayern e.V”.

Notes and references

- 1 Iijima, S. *Nature*, 1991, **354**, 56.
- 2 a) Li-Li, Y.; Kinloch, I.A.; Windle, A.H. *Science* 2004, **304**, 276. b) Nardecchia, S.; Carriazo, D.; Ferrer, M.L.; Gutierrez, M.C.; del Monte, F. *Chem. Soc. Rev.* 2013, **42**,794.

- 3 a) Wang, Z.; Mohammadzadeh, S.; Schmaltz, T.; Kirschner, J.; Khassanov, A.; Eigler, S.; Mundloch, U.; Backes, C.; Steinrück, H.-G.; Magerl, A.; Hauke, F.; Hirsch, A.; Halik, M. *ACS Nano* 2013, **7**, 11427. b) Avouris, P.; Chen, Z.; Perebeinos, V. *Nat. Nanotechnol.* 2007, **2**, 605. c) Park, H.; Afzali, A.; Han, S.-J.; Tulevski, G.S.; Franklin, A.D.; Tersoff, J.; Hannon, J.B.; Haensch, W. *Nat. Nanotechnol.*, 2012, **7**, 787.
- 4 Toma, F.M.; Sartorel, A.; Iurlo, M.; Carraro, M.; Parisse, P.; Maccato, C.; Rapino, S.; Rodriguez Gonzalez, B.; Amenitsch, H.; Da Ros, T.; Casalis, L.; Goldoni, A.; Marcaccio, M.; Scorrano, G.; Scoles, G.; Paolucci, F.; Prato, M.; Bonchio, M. *Nat. Chem.* 2010, **2**, 826.
- 5 a) Bartelmess, J.; Ballesteros, B.; de la Torre, G.; Kiessling, D.; Campidelli, S.; Prato, M.; Torres, T.; Guldi, D. M. *J. Am. Chem. Soc.* 2010, **132**, 16202. b) Campidelli, S.; Ballesteros, B.; Filoramo, A.; Diaz, D.D.; de la Torre, G.; Torres, T.; Rahman, G.M.A.; Ehli, C.; Kiessling, D.; Werner, F.; Sgobba, V.; Guldi, D.M.; Cioffi, C.; Prato, M.; Bourgoin, J.-P. *J. Am. Chem. Soc.* 2008, **130**, 11503. c) Ince, M.; Bartelmess, J.; Kiessling, D.; Dirian, K.; Martinez-Diaz, M. V.; Torres, T.; Guldi, D.M. *Chem. Sci.* 2012, **3**, 1472. d) Guldi, D.M.; Sgobba, V.; *Chem. Commun.* 2011, **47**, 606. e) Sandanayaka, A. S. D.; Maligaspe, E.; Hasobe, T.; Ito, O.; D'Souza, F. *Chem. Commun.* 2010, **46**, 8749. f) Das, S. K.; Subbaiyan, N. K.; D'Souza, F.; Sandanayaka, A. S. D.; Hasobe, T.; Ito, O. *Energy Environ. Sci.* 2011, **4**, 707. g) Dirian, K.; Herranz, A.M.; Katsukis, G.; Malig, J.; Rodriguez-Perez, L.; Romero-Nieto, C.; Strauss, V.; Martin, N.; Guldi, D.M. *Chem. Sci.* 2013, **4**, 4335.
- 6 Thess, A.; Lee, R.; Nikolaev, P.; Dai, H.; Petit, P.; Robert, J.; Xu, C.; Hee Lee, Y.; Gon, S.; Kim, A.; Rinzler, A. G.; Colbert, D. T.; Scuseria, G. E.; Tomanek, D.; Fischer, J. E.; Smalley, R. E. *Science* 1996, **273**, 483.
- 7 a) Hirsch, A. *Angew. Chem. Int. Ed.*, 2002, **41**, 1853. b) Jiang, C.; Saha, A.; Xiang, C.; Young, C. C.; Tour, J. M.; Pasquali, M.; Marti, A. A. *ACS Nano*, 2013, **7**, 4503. c) Singh, P.; Campidelli, S.; Giordani, S.; Bonifazi, D.; Bianco, A.; Prato, M. *Chem. Soc. Rev.* 2009, **38**, 2214. d) Hof, F.; Bosch, S.; Eigler, S.; Hauke, F.; Hirsch, A. *J. Am. Chem. Soc.* 2013, **135**, 18385.
- 8 a) Moore, V. C.; Strano, M.S.; Haroz, E. H.; Hauge, R. H.; Smalley, R. E. *Nano Lett.* 2003, **3**, 1379. b) O'Connell, M. J.; Bachilo, S.M.; Huffman, C. B.; Moore, V. C.; Strano, M. S.; Karoz, E. H.; Rialon, K.L.; Boul, P. J.; Noon, W. H.; Kitrell, C.; Ma, J.; Hauge, R.H.; Weizman, R. B.; Smalley, R. E. *Science*, 2002, **297**, 593. c) Matarredona, O.; Rhoads, H.; Li, Z.; Harwell, J.H.; Balzano, L.; Resasco, D.E. *J. Phys. Chem B* 2003, **107**, 13357.
- 9 a) Weil, T.; Vosch, T.; Hofkens, J.; Peneva, K.; Muellen, K. *Angew. Chem. Int. Ed.* 2010, **49**, 9068. b) Castellano, F.N. *Dalton Trans.*, 2012, **41**, 8493. c) Zhan, X.; Facchetti, A.; Barlow, S.; Marks, T. J.; Ratner, M. A.; Wasielewski, M. R.; Marder, S. R. *Adv. Mater.* 2011, **23**, 268.
- 10 a) Ehli, C.; Oelsner, C.; Guldi, D. M.; Mateo-Alonso, A.; Prato, M.; Schmidt, C.; Backes, C.; Hauke, F.; Hirsch, A. *Nature Chem.* 2009, **1**, 243. b) Oelsner, C.; Schmidt, C.; Hauke, F.; Prato, M.; Hirsch, A.; Guldi, D. M. *J. Am. Chem. Soc.* 2011, **133**, 4580.
- 11 Hu, Z.; Pantos, G. D.; Kuganathan, N.; Arrowsmith, R. L.; Jacobs, R. M. J.; Kociok-Köhn, G.; O'Byrne, J.; Jurkschat, K.; Burgos, P.; Tyrrell, R. M.; Botchway, S. M.; Sanders, J. K. M.; Pascu, S.I. *Adv. Funct. Mat.* 2012, **22**, 503.
- 12 a) Sakai, N.; Mareda, J.; Vauthey, E.; Matile, S. *Chem. Commun.* 2010, **46**, 4225. b) Bhosale, S. V.; Jani, C. H.; Langford, S. J. *Chem. Soc. Rev.*, 2008, **37**, 331. c) Guha, S.; Goodson, F.S.; Roy, S.; Corson, L. J.; Gravenmier, C. A.; Saha, S. *J. Am. Chem. Soc.* 2011, **133**, 15256. d) Guha, S.; Goodson, F.S.; Corson, L.J.; Saha, S. *J. Am. Chem. Soc.* 2012, **134**, 13679.
- 13 a) Imahori, H.; Yamada, H.; Guldi, D. M.; Endo, Y.; Shimomura, A.; Kundu, S.; Yamada, K.; Okada, T.; Sakata, Y.; Fukuzumi, S. *Angew. Chem. Int. Ed.*, 2002, **41**, 2344. b) El-Khouly, M. E.; Wijesinghe, C. A.; Nesterov, V. N.; Zandler, M. E.; Fukuzumi, S.; D'Souza, F. *Chem. Eur. J.* 2012, **18**, 13844. c) Banerji, N.; Bhosale, S. V.; Petkova, I.; Langford, S. J.; Vauthey, E. *Phys. Chem. Chem. Phys.*, 2011, **13**, 1019. d) Chaignon, F.; Falkenström, M.; Karlsson, S.; Blart, E.; Odobel, F.; Hammarström, L. *Chem. Commun.* 2007, 64. e) Hayes, R. T.; Wasielewski, M. R.; Gosztola, D. *J. Am. Chem. Soc.*, 2000, **122**, 5563. f) Liao, C.; Yarnell, J. E.; Glusac, K. D.; Schanze, K. S. *J. Phys. Chem. B.*, 2010, **114**, 14763.
- 14 a) Jentzsch, A. V.; Hennig, A.; Mareda, J.; Matile, S. *Acc. Chem. Res.*, 2013, **46**, 2791. b) Talukdar, P.; Bollot, G.; Mareda, J.; Sakai, N.; Matile, S. *J. Am. Chem. Soc.*, 2005, **127**, 6528. c) Bhosale, S.; Sisson, A.-L.; Talukdar, P.; Fürstenberg, A.; Banerji, N.; Vauthey, E.; Bollot, G.; Mareda, J.; Röger, C.; Würthner, F.; Sakai, N.; Matile, S. *Science* 2006, **313**, 84.
- 15 a) Kishore, R. S. K.; Kel, O.; Banerji, N.; Emery, D.; Bollot, G.; Mareda, J.; Gomez-Casado, A.; Jonkheijm, P.; Huskens, J.; Maroni, P.; Borkovec, M.; Vauthey, E.; Sakai, N.; Matile, S. *J. Am. Chem. Soc.*, 2009, **131**, 11106. b) Bhosale, R.; Misek, J.; Sakai, N.; Matile, S. *Chem. Soc. Rev.* 2010, **39**, 138. c) Lista, M.; Areephong, J.; Sakai, N.; Matile, S. *J. Am. Chem. Soc.* 2011, **133**, 15228.
- 16 Zhao, Y.; Beuchat, C.; Domoto, Y.; Gajewy, J.; Wilson, A.; Mareda, J.; Sakai, N.; Matile, S. *J. Am. Chem. Soc.* 2014, **136**, 2101.
- 17 a) Backes, C.; Hauke, F.; Hirsch, A. *Adv. Mat.* 2011, **23**, 2588. b) Backes, C.; Schmidt, C. D.; Hauke, F.; Böttcher, C.; Hirsch, A. *J. Am. Chem. Soc.* 2009, **131**, 2172.

- Journal Name** **ARTICLE**
- 18 Schmidt, C. D.; Böttcher, C.; Hirsch, A. *Eur. J. Org. Chem.*, 2007, 5497.
- 19 Pyrene in THF was utilized as standard.
- 20 a) Barros, T. C.; Brochsztain, S.; Toscano, V. G.; Filho, P. B.; Politi, M. J. *J.Photochem. Photobiol. A* 1997, **111**, 97. b) Andric, G.; Boas, J. F.; Bond, A. M.; Fallon, G. D.; Ghiggino, K. P.; Hogan, C. F.; Hutchinson, J. A.; Lee, M. A.-P.; Langford, S. J.; Pilbrow, J. R.; Troup, G. J.; Woodward, C. P. *Aust. J. Chem.*, 2004, **57**, 1011.
- 21 Green, S.; Fox, M.A. *J. Chem. Phys.* 1995, **99**, 14752.
- 22 Hurst, J.R.; McDonald, J. D.; Schuster, G. B. *J.Am.Chem.Soc.* 1982, **104**, 2065.
- 23 The redox potential of Fc/Fc⁺ was determined in a separate measurement and used as calibration for the silver wire acting as reference electrode.
- 24 Penneau, J.F.; Stallman, B. J.; Kasai, P. H.; Miller, L. L. *Chem. Mater.* 1991, **3**, 791.
- 25 Aveline, B.M.; Matsugo, S.; Redmond, R. W. *J.Am.Chem.Soc.* 1997, **119**, 11785.
- 26 a) Bachilo, S.M.; Strano, M.S.; Kitrell, C.; Hauge, R.H.; Smalley, R. E.; Weiszman, R. B. *Science* 2002, **298**, 2361. b) Duque, J.G.; Densmore, C.G.; Doorn, S.K. *J.Am.Chem.Soc.* 2010, **132**, 16165. c) Duque, J.G.; Parra-Vasquez, A.N.G.; Behabtu, N.; Green, M.J.; Higginbotham, A.L.; Price, B.K.; Leonard, A.D.; Schmidt, H.K.; Lounis, B.; Tour, J.M.; Doorn, S.K.; Cognet, L.; Pasquali, M. *ACS Nano* 2010, **4**, 3063.
- 27a) Dresselhaus, M. S.; Dresselhaus, G.; Saito, R.; Jorio, A. *Phys. Rep.* 2005, **409**, 47. b) Dresselhaus, M. S.; Jorio, A.; Hofmann, M.; Dresselhaus, G.; Saito, R. *Nano Lett.*, 2010, **10**, 751.
- 28 Schoeppler, F.; Ruehl, N.; Hertel, T. *Chem. Phys.* 2013, **413**, 112.
- 29 a) Carlson, L. J.; Krauss, T. D. *Acc. Chem. Res.* 2008, **41**, 235. b) Ostojic, G. N.; Zaric, S.; Kono, J.; Strano, M. S.; Moore, V. C.; Hauge, R. H.; Smalley, R. E. *Phys. Rev. Lett.*, 2004, **92**, 117402.
- 30 Backes, C.; Hauke, F.; Hirsch, A. *physica status solidi (b)*, 2013, **250**, 2592.
- 31 Backes, C.; Schmidt, C. D.; Rosenlehner, K.; Hauke, F.; Coleman, J. N.; Hirsch, A. *Adv. Mat.* 2010, **22**, 788.
- 32 a) Backes, C.; Mundloch, U.; Schmidt, C. D.; Coleman, J. N.; Wohlleben, W.; Hauke, F.; Hirsch, A. *Chem. Eur. J.* 2010, **16**, 13185. b) Backes, C.; Schmidt, C.D.; Hauke, F.; Hirsch, A. *Chem. Asian. J.* 2011, **6**, 438.
- 33 a) Ernst, F.; Heek, T.; Setaro, A.; Haag, R.; Reich, S. *Adv. Funct. Mater.* 2012, **22**, 3921. b) Ernst, F.; Heek, T.; Haag, R.; Reich, S.; Setaro, A. *physica status solidi (b)* 2012, **249**, 2465.
- 34 Crochet, J.; Clemens, M.; Hertel, T.; *J. Am. Chem. Soc.*, **2007**, **129**, 8058.
- 35 Romero-Nieto, C.; Garcia, R.; Herranz, M. A.; Rodriguez-Perez, L.; Sanchez-Navarro, M.; Rojo, J.; Martin, N.; Guldi, D. M. *Angew. Chem. Int. Ed.* 2013, **52**, 10216.
- 36 Paolucci, D.; Franco, M. M.; Iurlo, M. M.; Marcaccio, M.; Prato, M.; Zerbetto, F.; Penicaud, A.; Paolucci, F. *J. Am. Chem. Soc.* 2008, **130**, 7393.
- 37 a) Park, J.; Deria, P.; Therien, M. *J.Am.Chem.Soc.* 2011, **133**, 17156. b) Stich, D.; Spaeth, F.; Kraus, H.; Sperlich, A.; Dyakonov, V.; Hertel, T. *Nat. Photonics*, 2014, **8**, 139.